FAA-RD-81-44

Project Report
ATC-108

Coordinated Radar and Aircraft Observations of Turbulence

M. Labitt

26 May 1981

Lincoln Laboratory
MASSACHUSETTS INSTITUTE OF TECHNOLOGY
LEXINGTON, MASSACHUSETTS

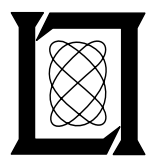

Prepared for the Federal Aviation Administration,
Washington, D.C. 20591

This document is available to the public through
the National Technical Information Service,
Springfield, VA 22161

Technical Report Documentation Page

1. Report No.	2. Government Accession No.	3. Recipient's Catalog No.
FAA-RD-81-44		

4. Title and Subtitle	5. Report Date
Coordinated Radar and Aircraft Observations of Turbulence	26 May 1981
	6. Performing Organization Code

7. Author(s)	8. Performing Organization Report No.
Melvin Labitt	ATC-108

9. Performing Organization Name and Address	10. Work Unit No. (TRAIS)
Massachusetts Institute of Technology Lincoln Laboratory P.O. Box 73 Lexington, MA 02173	11. Contract or Grant No. DTFA01-80-Y-10546
	13. Type of Report and Period Covered Project Report
12. Sponsoring Agency Name and Address Department of Transportation Federal Aviation Administration Systems Research and Development Service Washington, DC 20591	14. Sponsoring Agency Code ARD-231

15. Supplementary Notes

The work reported in this document was performed at Lincoln Laboratory, a center for research operated by Massachusetts Institute of Technology, under Air Force Contract F19628-80-C-0002.

16. Abstract

Interim results of a program to measure and correlate radar- and aircraft-sensed turbulence in rainstorms are presented. The dissipation factor of a turbulence air mass can be measured by an aircraft and a weather radar. Comparisons are made between precipitation reflectivity and spectral width measurements as indicators of turbulence. The instrumentation and data processing procedures are described. Examples of turbulence observations made with a storm-penetrating aircraft and the weather radar are given. The relationship between the radar observations and the physical properties of the turbulence atmosphere are derived. The relationship of radar spectral width (variance) to turbulence intensity is discussed.

17. Key Words	18. Distribution Statement
Air Traffic Control Weather Radar Sensing Aircraft sensing of turbulence Turbulence Weather radar velocity variance/ spectral width Dissipation factor Universal turbulence intensity scale Weather radar intensity	Document is available to the public through the National Technical Information Service, Springfield, Virginia 22161

19. Security Classif. (of this report)	20. Security Classif. (of this page)	21. No. of Pages	22. Price
Unclassified	Unclassified	44	

Form DOT F 1700.7 (8-72) Reproduction of completed page authorized

ENGLISH/METRIC CONVERSION FACTORS

LENGTH

From \ To	cm	m	km	in	ft	mi	nmi
cm	1	0.01	$1x10^{-5}$	0.3937	0.0328	$6.21x10^{-6}$	$5.39x10^{-6}$
m	100	1	0.001	39.37	3.281	0.0006	0.0005
km	100,000	1000	1	39370	3281	0.6214	0.5395
in	2.540	0.0254	$2.54x10^{-5}$	1	0.0833	$1.58x10^{-5}$	$1.37x10^{-5}$
ft	30.48	0.3048	$3.05x10^{-4}$	12	1	$1.89x10^{-4}$	$1.64x10^{-4}$
mi	160,900	1609	1.609	63360	5280	1	0.8688
nmi	185,200	1852	1.852	72930	6076	1.151	1

AREA

From \ To	cm^2	m^2	km^2	in^2	ft^2	mi^2	nmi^2
cm^2	1	0.0001	$1x10^{-10}$	0.1550	0.0011	$3.86x10^{-11}$	$5.11x10^{-11}$
m^2	10,000	1	$1x10^{-6}$	1550	10.76	$3.86x10^{-7}$	$5.11x10^{-7}$
km^2	$1x10^{10}$	$1x10^{6}$	1	$1.55x10^{9}$	$1.08x10^{7}$	0.3861	0.2914
in^2	6.452	0.0006	$6.45x10^{-10}$	1	0.0069	$2.49x10^{-10}$	$1.88x10^{-10}$
ft^2	929.0	0.0929	$9.29x10^{-8}$	144	1	$3.59x10^{-8}$	$2.71x10^{-8}$
mi^2	$2.59x10^{10}$	$2.59x10^{6}$	2.590	$4.01x10^{9}$	$2.79x10^{7}$	1	0.7548
nmi^2	$3.43x10^{10}$	$3.43x10^{6}$	3.432	$5.31x10^{9}$	$3.70x10^{7}$	1.325	1

VOLUME

From \ To	cm^3	liter	m^3	in^3	ft^3	yd^3	fl. oz.	fl. pt.	fl. qt.	gal.
cm^3	1	0.001	$1x10^{-6}$	0.0610	$3.53x10^{-5}$	$1.31x10^{-6}$	0.0338	0.0021	0.0010	0.0002
liter	1000	1	0.001	61.02	0.0353	0.0013	33.81	2.113	1.057	0.2642
m^3	$1x10^{6}$	1000	1	61,000	35.31	1.308	33,800	2113	1057	264.2
in^3	16.39	0.0163	$1.64x10^{-5}$	1	0.0006	$2.14x10^{-5}$	0.5541	0.0346	2113	0.0043
ft^3	28,300	28.32	0.0283	1728	1	0.0370	957.5	59.84	0.0173	7.481
yd^3	765,000	764.5	0.7646	46700	27	1	25900	1616	807.9	202.0
fl. oz.	29.57	0.2957	$2.96x10^{-5}$	1.805	0.0010	$3.87x10^{-5}$	1	0.0625	0.0312	0.0078
fl. pt.	473.2	0.4732	0.0005	28.88	0.0167	0.0006	16	1	0.5000	0.1250
fl. qt.	948.4	0.9463	0.0009	57.75	0.0334	0.0012	32	2	1	0.2500
gal.	3785	3.785	0.0038	231.0	0.1337	0.0050	128	8	4	1

MASS

From \ To	g	kg	oz	lb	ton
g	1	0.001	0.0353	0.0022	$1.10x10^{-6}$
kg	1000	1	35.27	2.205	0.0011
oz	28.35	0.0283	1	0.0625	$3.12x10^{-5}$
lb	453.6	0.4536	16	1	0.0005
ton	907,000	907.2	32,000	2000	1

TEMPERATURE

$°C = 5/9 (°F - 32)$

$°F = 9/5 (°C) + 32$

COORDINATED RADAR AND AIRCRAFT OBSERVATIONS OF TURBULENCE

1.0 INTRODUCTION

The ability to sense and display regions of hazardous turbulence aloft is an essential prerequisite to the selection of safe, minimum-distance-traveled flight paths. Lincoln Laboratory, under a program sponsored by the Federal Aviation Administration, has undertaken to measure and correlate radar- and aircraft-sensed turbulence in rainstorms.* This paper presents interim results of these measurements. Results of the measurements are expected to provide guidance in the design of equipment that will display areas of hazardous turbulence with confidence. Plots of turbulence levels measured simultaneously by a ground radar and an aircraft are shown to illustrate the correlation. Comparisons of the turbulence levels with the rain reflectivity are also made.

2.0 BACKGROUND

Precipitation reflectivity and spectral width as measured by a ground-based weather radar have been used as turbulence indicators. The current research focuses on an investigation of the use of spectral width as a reliable indicator of turbulence in precipitation.

The dissipation factor, ε, of the turbulent air mass can be measured by both the aircraft and the radar and is independent of type and speed of the aircraft and of the radar parameters. The dissipation factor, as used in turbulence theory, represents the kinetic energy converted to heat per unit mass per unit time. This conversion to heat occurs at the end of the sequence where the large eddies progressively decay into smaller and smaller eddies. The conversion from kinetic to thermal energy occurs on the scale of millimeters. MacCready[3] has related ε to the response of a particular aircraft as well as to a universal turbulence intensity scale.

---

*This work is an extension of the work reported in Reference 1 and is noted in Reference 2.

The quantity ε can be determined directly by the aircraft by simply measuring the fluctuations in instantaneous airspeed. Kolmogorov[4] has shown that the structure function of the instantaneous airspeed $D_v = C(\varepsilon r)^{2/3}$, where D_v is defined as the average of the square of the difference of two successive airspeeds v measured a distance r apart. It is assumed that homogeneous isotropic turbulence exists.

$$D_v = E\{(v_2 - v_1)^2\} = C(\varepsilon r)^{2/3}$$

The universal constant C has been experimentally determined to be $1.77 \pm .08$. It can also be shown (see Appendix A) that the acceleration* an aircraft experiences is proportional to $\varepsilon^{1/3}$, i.e.,

$$\sqrt{D_a} = KC^{1/2} \rho\varepsilon^{1/3} \frac{v^{4/3}}{m}$$

Here ρ is the air density, v is the air-craft speed, m is the aircraft mass and K is a constant of proportionality unique for a particular aircraft. It is obvious from the above relations that the quantity $\varepsilon^{1/3}$ rather than ε itself is the more useful quantity.

The ground-based radar can also determine $\varepsilon^{1/3}$ from measurements of the width of the rainstorm radar spectrum. If it is assumed as before that the turbulence is isotropic and homogeneous, then the following relation between $\varepsilon^{1/3}$ and the spectral width σ_u holds:[5]

$$\sigma_u^2 = \Gamma(\tfrac{2}{3})\alpha(\varepsilon a)^{2/3} F(-\tfrac{1}{3}, \tfrac{1}{2}; \tfrac{5}{2}; 1 - \tfrac{b^2}{a^2})$$

where $a > b$ [1]

*Actually the square root of the acceleration structure function.

The parameters above are defined as follows:

$\Gamma(\frac{2}{3})$ = gamma function (1.35411--)
α = universal constant (1.35 $\pm$ .06)
a = radar half beamwidth (cm)
b = radar half pulse length (cm)
F = Gaussian hypergeometric function
ε = dissipation factor ($cm^2 sec^{-3}$)

It is shown in Appendix B that equation [1] can be closely approximated by

$$\sigma_u^2 \approx \Gamma(\frac{2}{3})\alpha(\varepsilon a)^{2/3} = 1.828(\varepsilon a)^{2/3} \qquad [2]$$

Notice that Eqs. [1] and [2] do not contain an unknown constant of proportionality. It is for this reason that the initial emphasis has been to measure turbulence in terms of the spectral width rather than some other parameter such as velocity gradient where an equivalent theoretical relationship is not available.

3.0 EQUIPMENT DESCRIPTION

The basic experiment consists of flying an instrumented aircraft through a turbulent rainstorm while, at the same time, the ground-based instrumentation radar attempts to estimate the amount of turbulence ($\varepsilon^{1/3}$) present via an appropriate algorithm. One of the objects of this program is to determine the best radar operating parameters and algorithms to use. A brief description of the aircraft and radar instrumentation follows.

3.1 Aircraft Equipment

An instrumented, twin engine, turboprop Grumman Gulfstream, operated by the FAA Technical Center was used to penetrate storm cells under surveillance by the ground-based radar. Within the storm cells the aircraft sensed $\varepsilon^{1/3}$ by measuring the pitot differential pressure referenced to static pressure (IAS); outside total temperature, and absolute pressure (barometric altitude) were also measured. In addition, the aircraft carried a vertical accelerometer mounted at the center of gravity of the aircraft to provide a measure of relative turbulence level, an inertial navigation system to provide the

aircraft position, and a time-of-day clock. All of the sensor outputs are digitally recorded on tape with a 1 second update rate with the exception of the pitot pressure and the accelerometer outputs which are sampled 100 and 20 times per second respectively.

3.2 Ground Equipment

The ground-based facilities included, in addition to the instrumentation radar, a radar beacon interrogator and a station-keeping radar which were used respectively for the control of the aircraft and for the location of storms. The instrumentation radar consisted of an S-band ASR-8 coherent transmitter with its front end coupled to a 15-foot parabolic antenna mounted on a digitally controlled pedestal. A custom-built receiver consisting of a linear IF strip drives a pair of quadrature detectors which in turn drive 10-bit A/D converters. The output of the A/D converters fills a fast 256K by 20-bit buffer during a sector scan of the antenna. The data is then read out on tape via a NOVA computer. The antenna has a 1.6-degree one-way beamwidth and is capable of being pointed in azimuth or elevation either manually or by computer control.

An ATCBI-4 beacon radar is used to locate the aircraft. Its antenna has a 2.4-degree azimuthal beamwidth, is mounted on the station keeping radar antenna, and is located 30 meters from the instrumentation radar.

The station-keeping radar is an FAA S-band ASR-7 terminal radar connected to a ASR-5 fan-beam antenna. Its output is presented on a PPI to locate storms. The instrumentation radar cannot be easily used for this purpose.

A Data Entry 2nd Display System (DEDS) presents both analog video and alphanumeric characters on a PPI-like display. Normal video from the station keeping radar and the beacon returns are presented as analog video. NOVA-processed data such as dBz level, mean radial velocity, turbulence levels ($\epsilon^{1/3}$) as well as the most recent minute's worth of beacon returns are superimposed as alphanumerics. This allows the operator to determine in real-time whether a particular area is hazardous and should be avoided, or whether it should be penetrated by the instrumented aircraft to gather data.

4.0 CALIBRATION AND ERROR ASSESSMENT

Sources of error in the experiments requiring special attention were:

a. Beacon Antenna Pointing (AZ)

b. Instrumentation Antenna Pointing (AZ + EL)

c. Instrumentation Radar and Antenna Gain

d. Beacon Range Error

e. Synchronization of Aircraft and Radar Clocks

Beacon antenna pointing was calibrated by observing a transponder on the ground whose position is known relative to the radar. The Instrumentation Antenna pointing was calibrated by directing the antenna to an accurately calculated position of the sun. By noting how far the antenna has to be moved to be precisely on boresight with the sun it was found that the error was small, less than 0.1 degree over a period of approximately six hours. The Instrumentation Radar antenna gain was determined by measuring the solar flux level when observing the sun and comparing it with the published values for that time and day. The radar receiver gain was determined by injecting a calibrated noise source into the radar waveguide directional coupler. A fixed beacon range error of 0.26 nmi was found when comparing simultaneous observation of the aircraft by the instrumented radar and the beacon. The error is attributed to the differences in delay between the ground and aircraft beacon transponders and has been removed. It is obvious that the ground instrumentation computer clock must be carefully synchronized by the aircraft instrumentation clock. This is done before takeoff and rechecked several times during the flight by voice communication. The timing should be better than one second accuracy and should not cause any appreciable error in the overall results.

5.0 DATA REDUCTION PROCEDURES

5.1 Beacon Algorithm

The purpose of the beacon data reduction algorithm is to accurately locate the instrumented aircraft relative to the storm. However, when the beacon data was taken, it was found that some of the data was contaminated by spurious returns from other aircraft having the same code, from the ground

test transponder, and from undetected errors in the NOVA program. The errors have been corrected, however, since the data is valuable. A successful effort has been made to retrieve the contaminated data.

Fig. 1a shows a plot of the raw beacon returns from the July 3 flight. Returns from the ground have already been removed. The wide scatter is primarily due to the old error in the NOVA program that considers returns in adjacent range gates as separate targets. As a result of this, a corrective program was written to cluster the returns on the basis that any returns within a certain area and time box are the same. The results are shown in Fig. 1b. Any missing returns are then filled in using a fourth order least square fit. Missing points have been caused by propagation effects such as the orientation of the aircraft or flying in the cone of silence of the beacon radar. Other causes of missing returns have been an error in the NOVA program (which has been since corrected) and possible mixups in the settings of the data collection equipment. Filling in the missing points is needed to allow proper smoothing in those areas adjacent to the missing points. Fig. 1c shows the missing points replaced while Fig. 1d has been smoothed and interpolated. The smoothing and interpolation is accomplished using a Fast Fourier Transform (FFT) technique. The x and y components of the beacon track are Fourier-transformed, zeros are added to the high frequency end so that the total number of FFT points are increased by four, the transform is then multiplied by a Gaussian weighting function, the inverse transform is then taken, resulting in a smoothed beacon track with four times as many points. Rather than having a beacon file with an update of 4.8 seconds, it is now every 1.2 seconds and will allow a smoother merging with the instrumentation radar data.

5.2 Instrumentation Radar Algorithms

The instrumentation radar records on tape the unprocessed radar data as an in-phase and quadrature component for each of the range-azimuth cells in a selected sector. The tapes are then sent to Lincoln Laboratory for processing in the following manner. The raw data, which represent the returns from

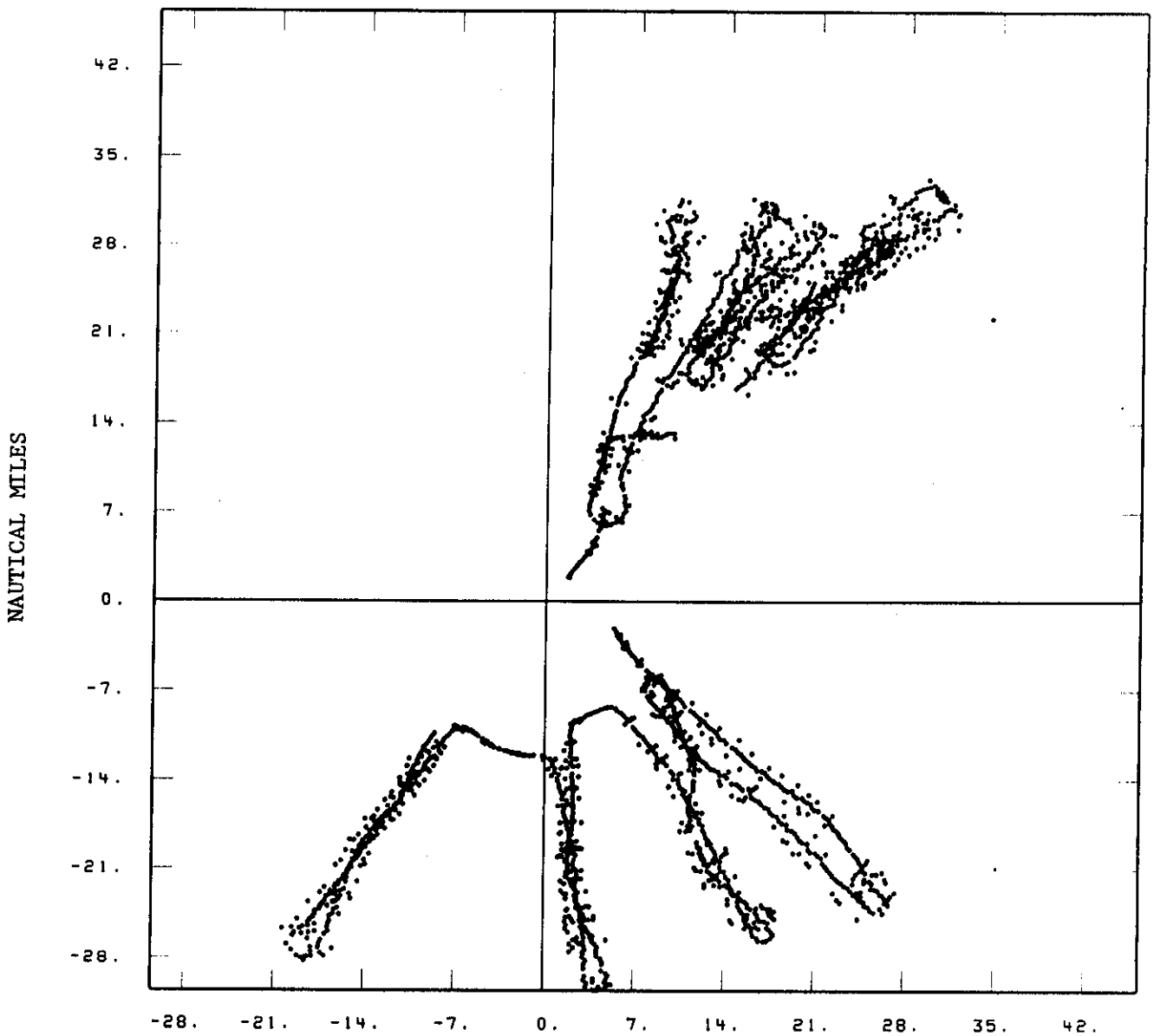

Fig. 1a. Raw beacon returns from July 3, 1980 flight.

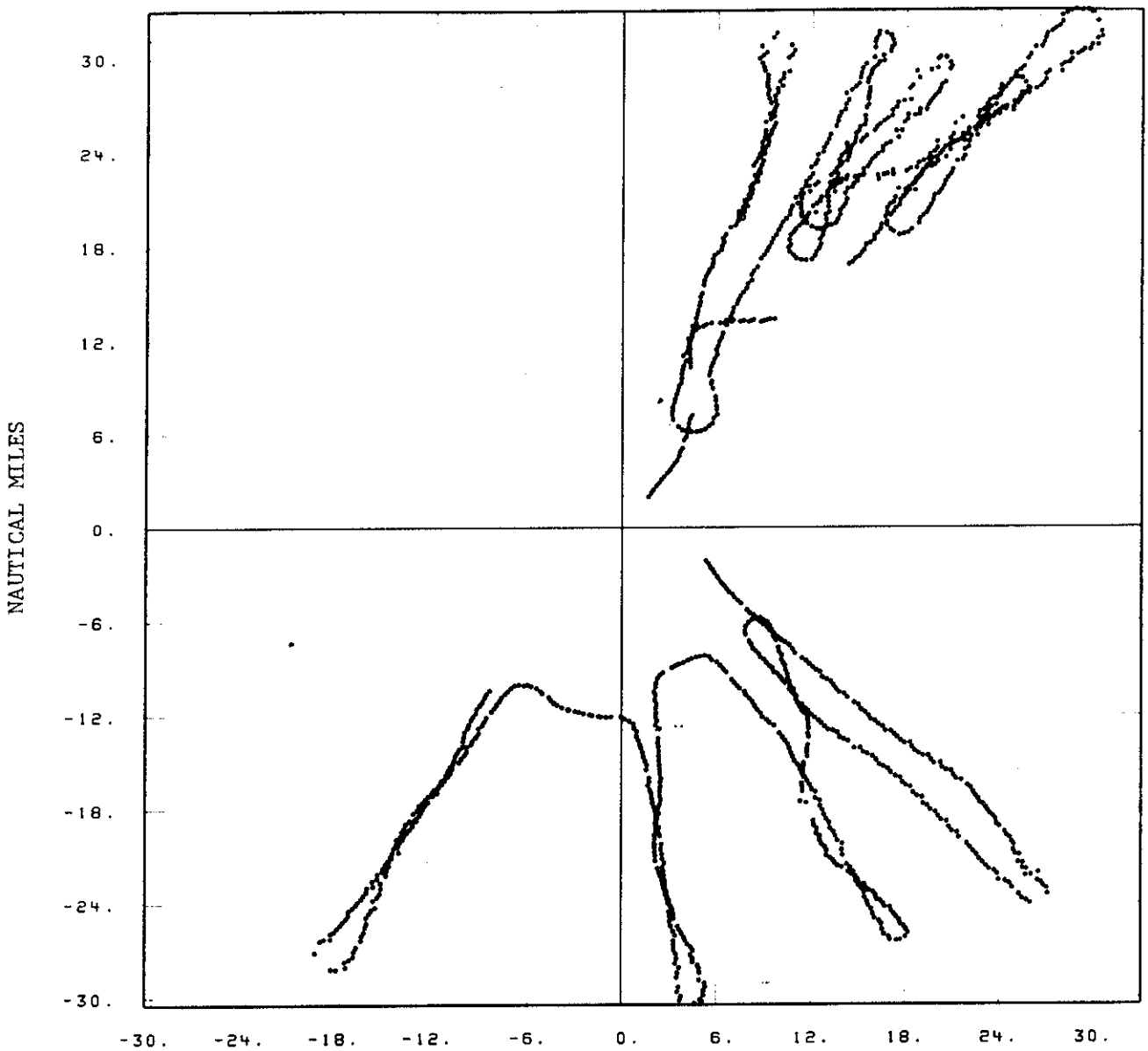

Fig. 1b. Clustered beacon returns.

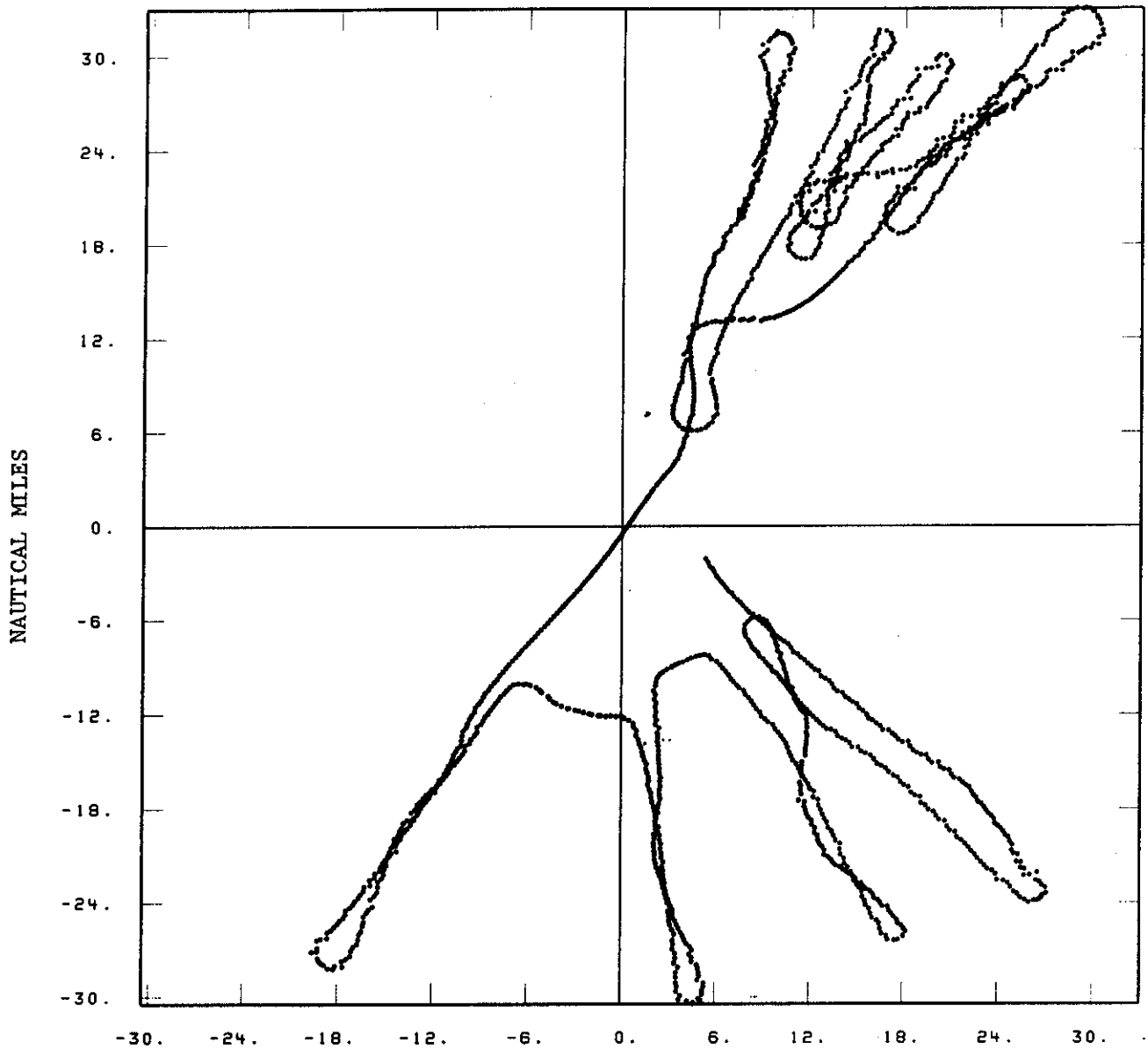

Fig. 1c. Missing returns filled in.

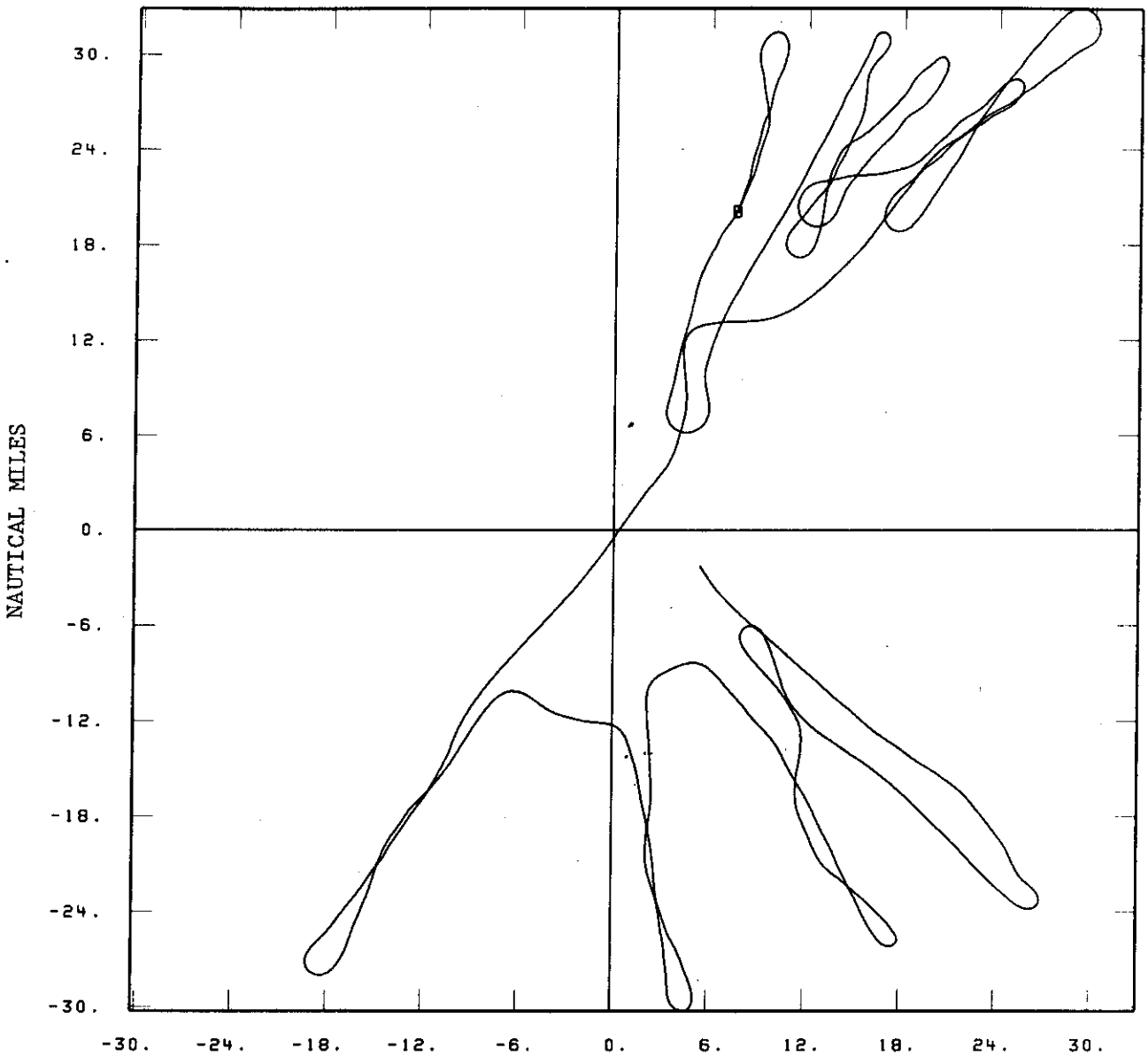

Fig. 1d. Smoothed and interpolated.

the rain droplets, were recorded range sequentially. However, the processing requires that the data be first reordered in azimuth. A maximum entropy estimation is then made of the autocorrelation lags. The lags are used in the computation of moments. The moments, in turn, provide, by using specific pulse pair algorithms, the intensity (dBz), the mean radial velocity, and the spectral width (in $\epsilon^{1/3}$ units). The maximum entropy estimation of the lags is used because it provides a better estimate than a straightforward calculation. This is because the entropy calculation requires that the estimated correlation lags be consistent with one another (this insures that the spectra the lags represent are positive for all frequencies). A set of autocorrelation lags are computed for each radar cell. Typically each cell is made up of 204 returns (I and Q components). The expressions for converting the correlation lags to moments are as follows:

Intensity or 0-th moment:

$$dBz = 10 \log(k|R_o|) \qquad [3a]$$

Mean radial velocity or 1st moment:

$$v = \frac{\lambda}{4\pi T} \tan^{-1}\left(\frac{I_m(R_1)}{R_e(R_1)}\right) \qquad [3b]$$

Velocity variance or 2nd moment:

$$\sigma_v^2 = \frac{\lambda^2}{24\pi^2 T^2} \ln \frac{|R_1|}{|R_2|} \qquad [3c]$$

where R_n is the n'th autocorrelation lag, λ the radar wavelength, T is the interpulse period, and k a constant determined from the radar parameters. The

above algorithms are subject to a minimum signal-to-noise value. In particular, the 2nd moment estimator requires at least a 3 dB S/N. The S/N estimator used is

$$\frac{S}{N} = 1/\left(\frac{R_o R_2^{1/3}}{R_1^{4/3}} - 1\right).$$

The 2nd moment and S/N estimators were derived assuming the spectra is Gaussian-shaped. Monte Carlo tests of these estimators show that the algorithms are valid for a time series that has a Gaussian-shaped spectrum. Homogeneous isotropic turbulence theoretically is expected to produce a Gaussian-shaped radar spectrum.

The computations produce arrays of numbers that represent the moments at relatively coarse discrete uniform positions over the recorded sector area. In the azimuth dimension they are a beamwidth apart while in range they are spaced 112.5, 225 or 450 meters. Consequently, quantization occurs when one attempts to assign a value to the moments along the aircraft track. Smoothing and interpolating these discrete points is accomplished using a two-dimensional FFT procedure. Fig. 2 and Fig. 3 are contour plots that were processed in this manner. Superimposed are the aircraft tracks. In general the tracks extend in time halfway to the previous scan time to halfway to the next scan time. Comparing dBz and $\varepsilon^{1/3}$ contours for the same scan, it is clear that the $\varepsilon^{1/3}$ contours are much more structured. The intensity plots are smooth and featureless compared to the widths ($\varepsilon^{1/3}$). The $\varepsilon^{1/3}$ contours on the right side have low spectral widths, which imply low turbulence levels while the left side indicates that there are areas of strong turbulence. In contrast, the intensity contours give no indication of heavy turbulence on the left side. Comparisons with the aircraft data will be discussed later.

5.3 Aircraft Data Reduction

The effect of turbulence on the pitot-equipped aircraft is sensed by measuring the rms acceleration and the dissipation factor. The acceleration

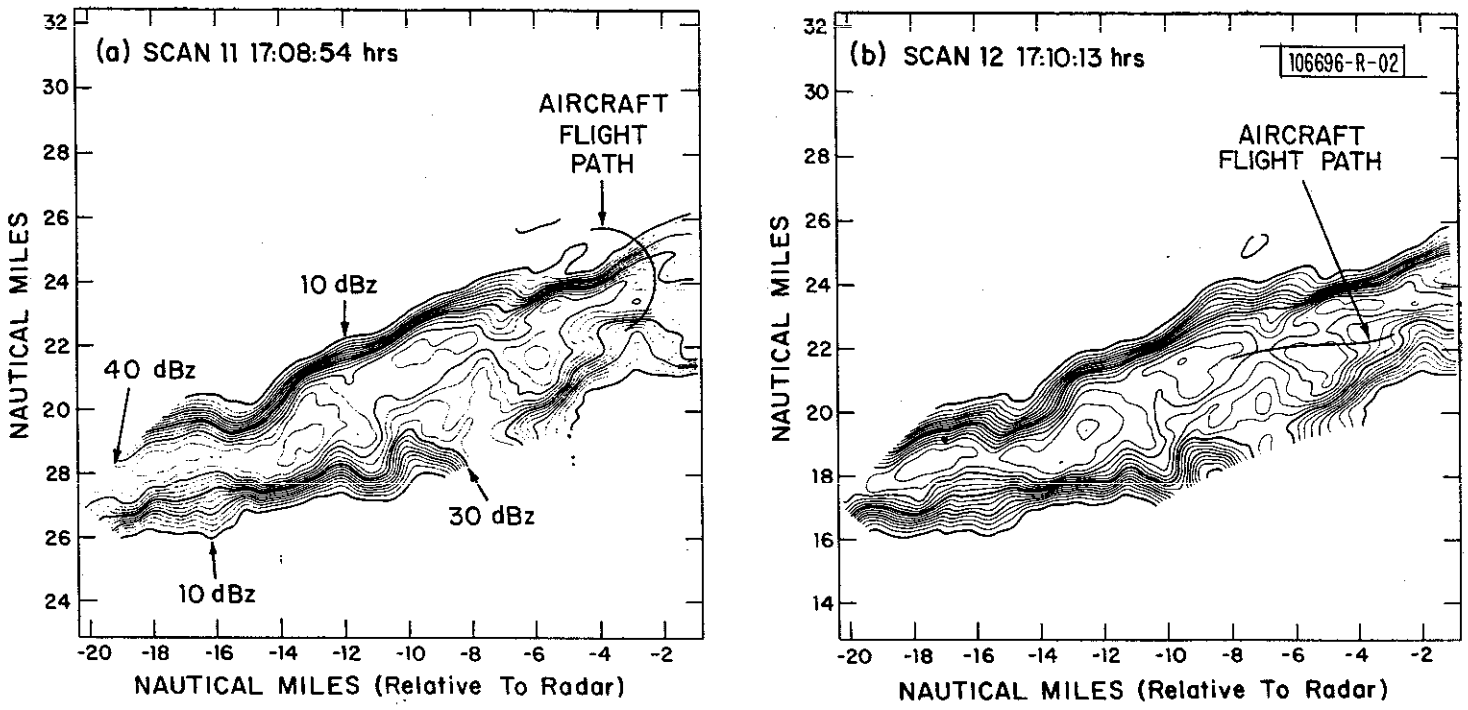

Fig. 2. (a-b) Reflectivity contours (dBz) in 2-dB steps. (Flight of 17 July 1980).

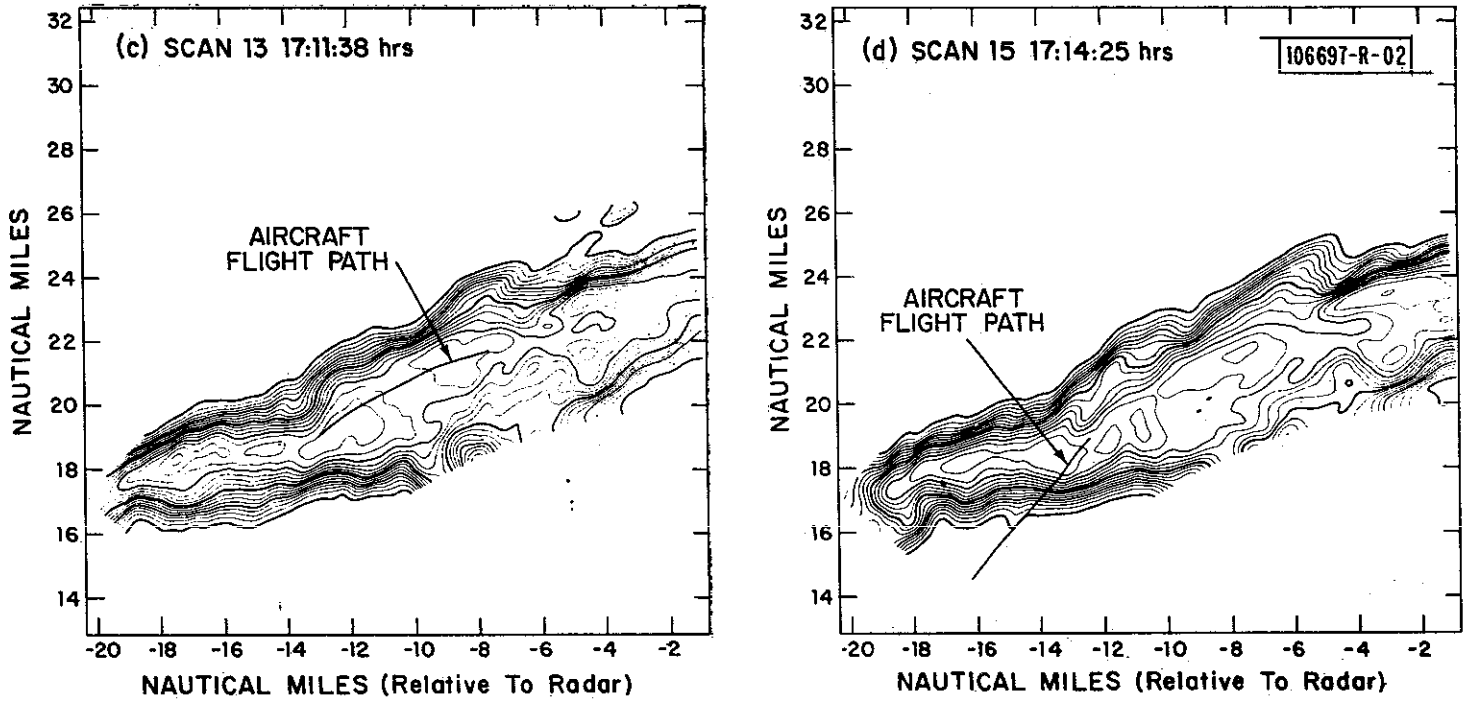

Fig. 2. (c-d) Reflectivity contours (dBz) in 2-dB steps. (Flight of 17 July 1980).

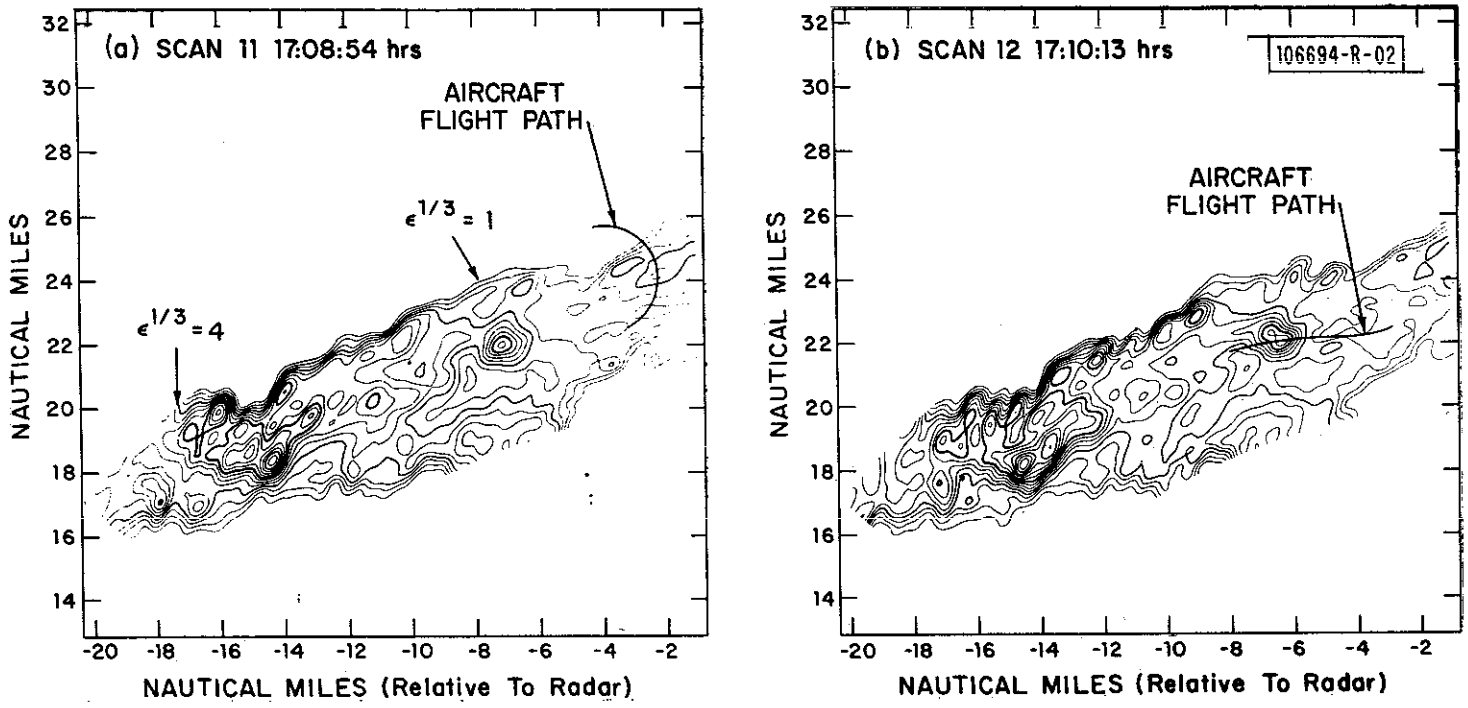

Fig. 3. (a-b) Contours of $\epsilon^{2/3}$ ($cm^{2/3} sec^{-1}$) in unity steps (Flight of 17 July 1980).

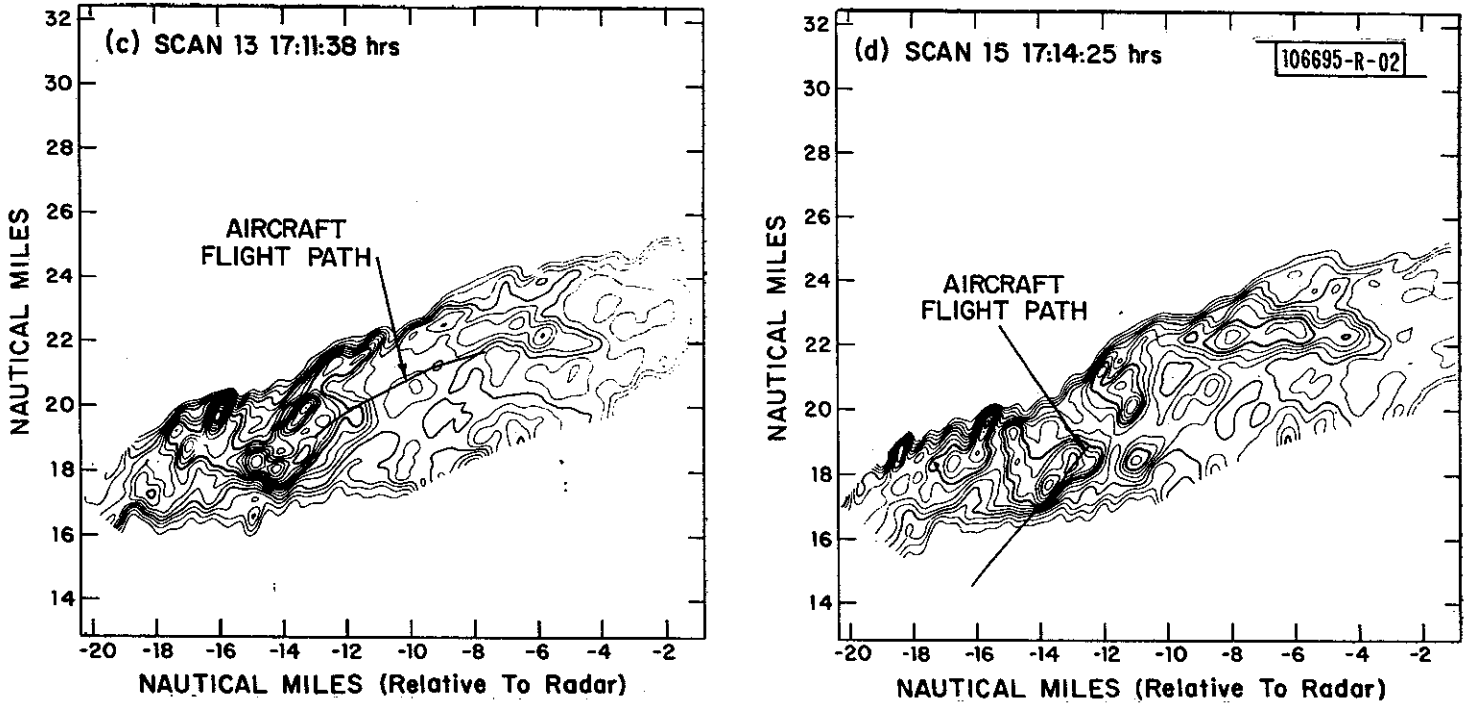

Fig. 3. (c-d) Contours of $\varepsilon^{2/3}(cm^{2/3}sec^{-1})$ in unity steps (Flight of 17 July 1980).

is measured directly. The dissipation factor ε is found from the pitot differential pressure Δp, the total (stagnation) temperature T_t and the absolute pressure P_f (free stream pressure or barometric altitude), and is as follows:

$$\varepsilon^{1/3} = \frac{\left(\frac{RT_t}{\tau}\right)^{1/3} \left(\frac{\gamma-1}{2\gamma}\right)^{2/3} \sqrt{D_{\Delta p}}}{C^{1/2}\left(1 + \frac{\Delta p}{P_f}\right)^{\frac{\gamma+2}{3\gamma}} \left[\left(1 + \frac{\Delta p}{P_f}\right)^{\frac{\gamma-1}{\gamma}} - 1\right]^{2/3} P_f} \qquad [4]$$

where the Δp structure function is defined as

$$D_{\Delta p} \triangleq E\{(\Delta p(t + \tau) - \Delta p(\tau))^2\},$$

$R = 2.87 \times 10^6 \left(\frac{cm}{sec}\right)^2 K^{-1}$ gas constant,

$\gamma = 1.4$ ratio of specific heats,

$\tau = 0.2\text{-}1.0$ (sec) time between successive Δp measurements,

and $C = 1.77$ Kolmogorov's constant.

Eq. [4] takes into account the aircraft altitude, airspeed and Mach number. Both the structure function and the aircraft rms vertical acceleration are continuously averaged over a 7.5 second period using a cosine squared weighting. Examples of time plots of $\varepsilon^{1/3}$ and rms acceleration are shown in the upper and middle curves of Figs. 4 through 7.

6.0 COMPARISON OF AIRCRAFT AND RADAR DATA

The lower curves of Fig. 4 and 5 are the values of $\varepsilon^{1/3}$ measured by the radar using Eqs. [2] and [3]. This is of the July 17, 1980 flight and will be examined at length here because it includes cases where the aircraft passed through low- and high-turbulence areas. The aircraft made many passes at a 5,000 ft. altitude through a moderately violent thunderstorm in the Atlantic City area. Many other flights have been examined but not in as much detail. Figs. 6 and 7 are of the corresponding reflectivity in dBz. The numbered dots above the radar data (lower curve) represent the midpoint time when a particular radar scan (or snapshot) was taken. If the aircraft is in a radar cell, it will appear at this time. The smallest value of reflectivity that can be measured with the radar is 8 dBz. However, it is felt that in order to trust the width algorithms (radar $\varepsilon^{1/3}$) the reflectivity should be greater than 14 dBz.

The time interval 17:08 to 17:15 Fig. 4 exhibits a reasonable correlation between radar and aircraft $\varepsilon^{1/3}$ while the corresponding reflectivity Fig. 6 does not. The radar peak at 17:09 is contaminated by the aircraft. A spectral analysis of the radar return at this time, range and azimuth show the aircraft to be present. The peak at scan 12 (17:10:30) is real (no aircraft) and correlates with the rms acceleration and the aircraft $\varepsilon^{1/3}$. A scatter plot has been generated over this time interval and is shown in Fig. 8a. Here the aircraft $\varepsilon^{1/3}$ is compared to the radar $\varepsilon^{1/3}$. A reasonable correlation is evident. The corresponding correlation coefficient is 0.81. The correlation with reflectivity (Fig. 8b) is 0.57. If the entire flight of 17 July 1980 is used, then the correlation is 0.50 using spectral width ($\varepsilon^{1/3}$) and 0.29 using reflectivity. The respective scatter plots are shown in Fig. 8c and 8d. In this calculation the data was edited to remove those parts that were known to be contaminated by the aircraft. For example, at time 17:47, scan 39, the large lobe is due to the aircraft in a range cell. See Fig. 5. Fig. 9a and 9b show the interval 17:18 to 17:31. The width correlation is 0.48 while the reflectivity is 0.10. This data includes the large anomalous $\varepsilon^{1/3}$ peak at 17:30:10.

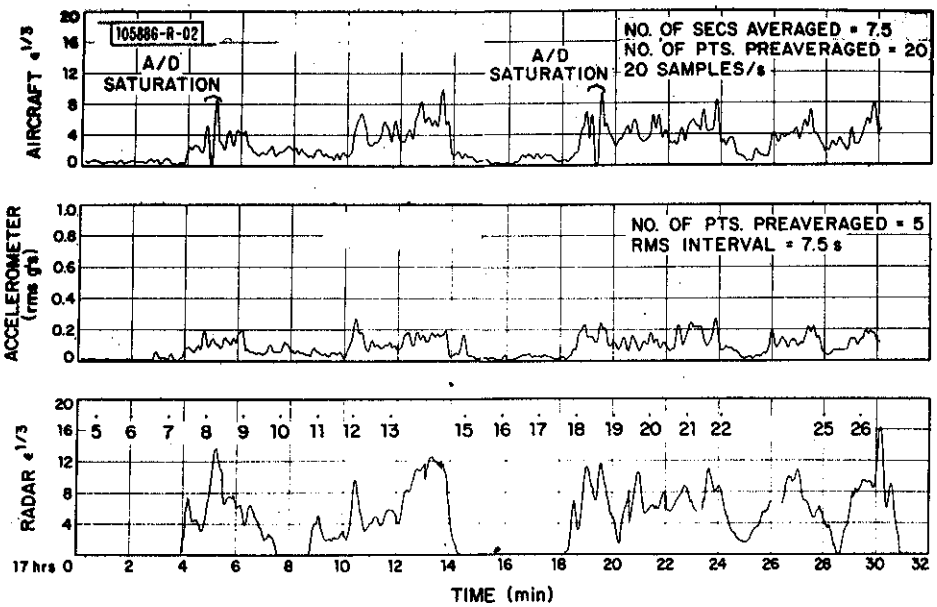

Fig. 4. Comparison of radar $\varepsilon^{1/3}$ (bottom curve) with aircraft $\varepsilon^{1/3}$ (top curve) and aircraft rms acceleration (middle curve). (Flight of 17 July 1980).

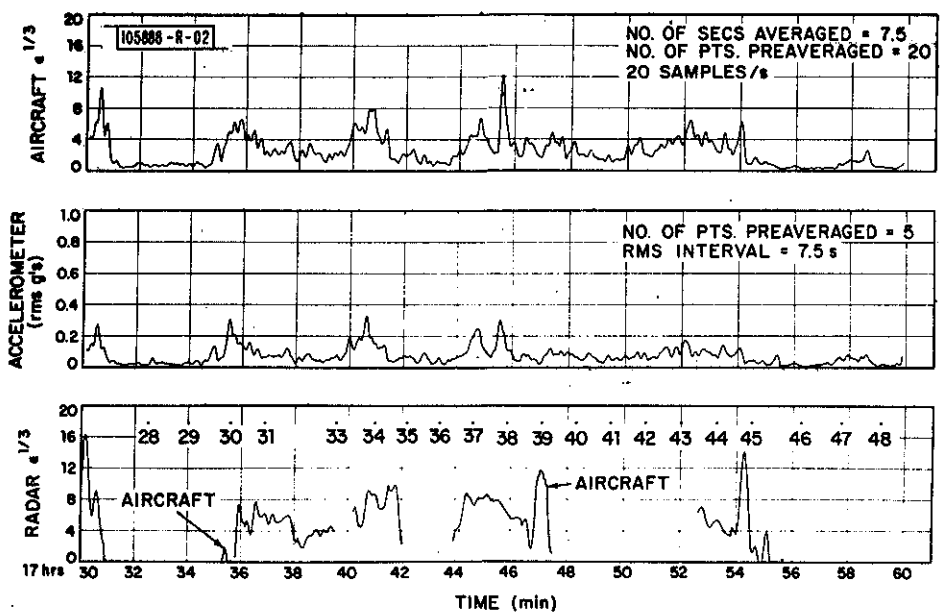

Fig. 5. Continuation of curves of Fig. 4.

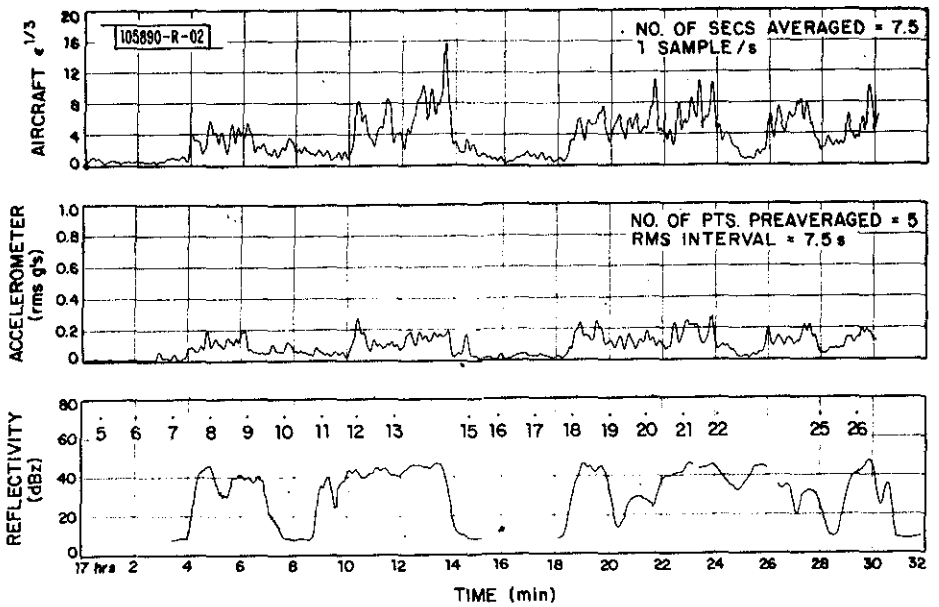

Fig. 6. Comparison of radar reflectivity (bottom curve) with aircraft $\varepsilon^{1/3}$ (top curve) and aircraft rms accelaration (middle curve). (Flight of 17 July 1980).

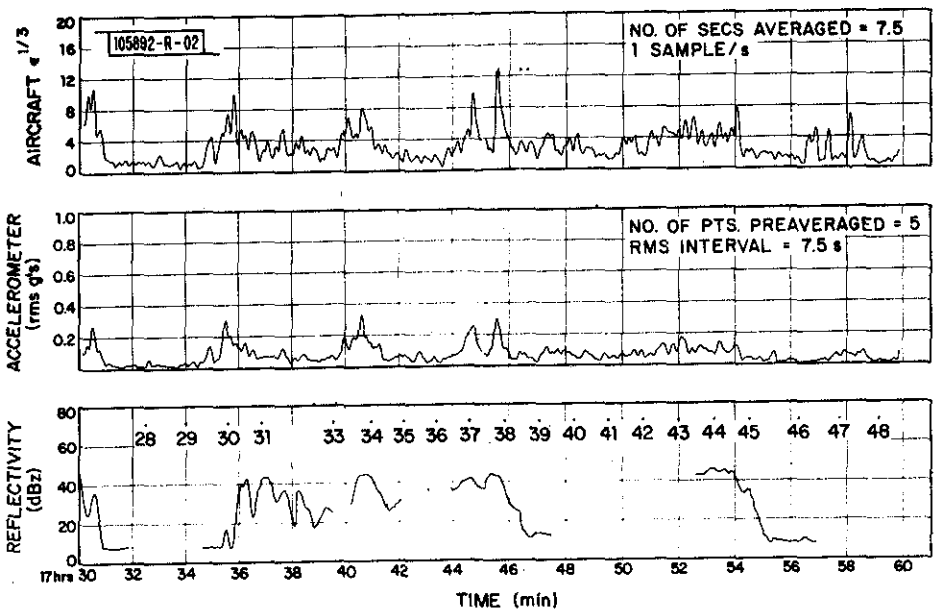

Fig. 7. Continuation of curves of Fig. 6.

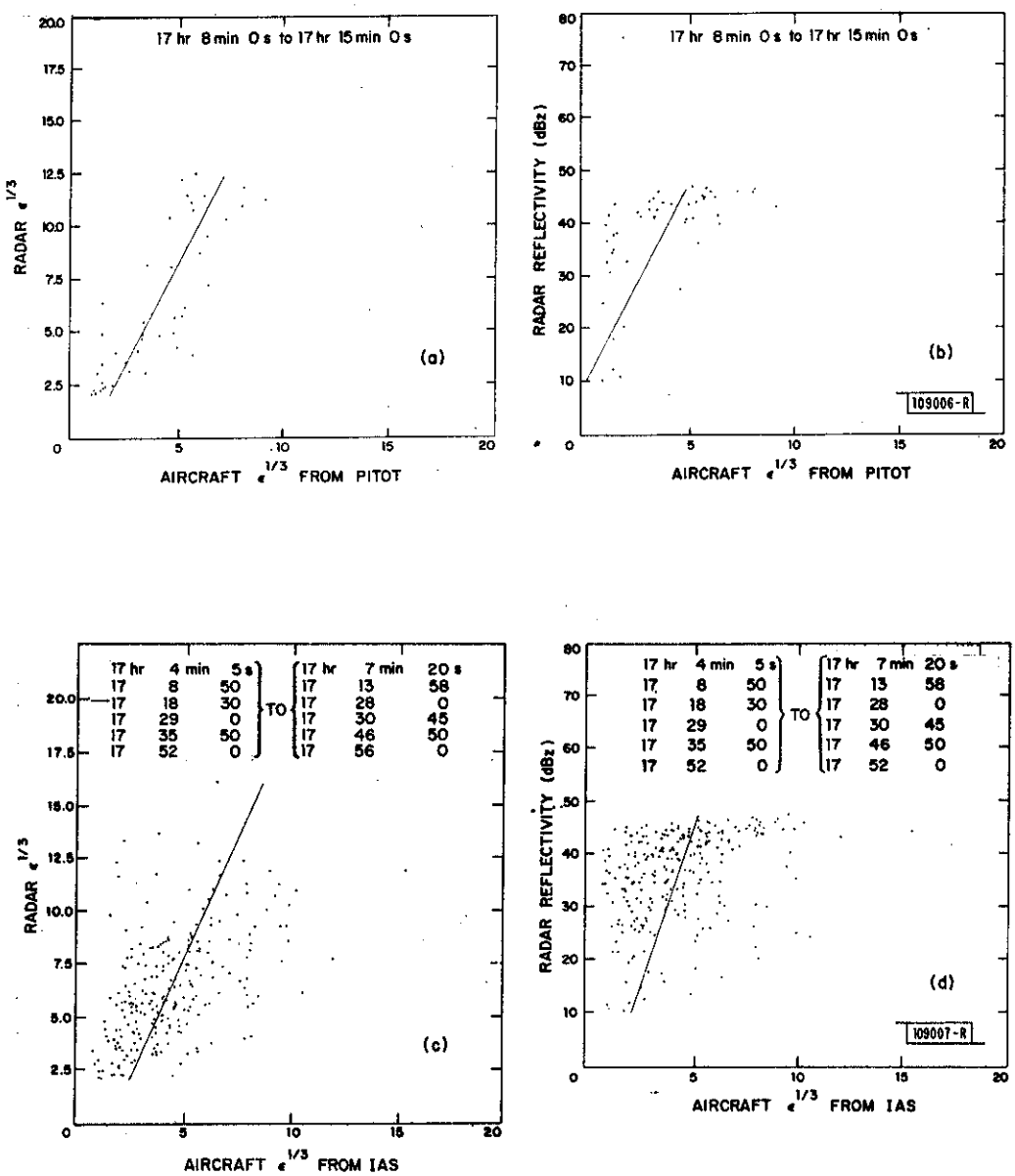

Fig. 8. (a-d) Scatter plots of radar $\varepsilon^{1/3}$ and reflectivity vs aircraft $\varepsilon^{1/3}$. (Flight of 17 July 1980). (a) Correlation coefficient = 0.81, (b) correlation coefficient = 0.57, (c) correlation coefficient = 0.50, (d) correlation coefficient = 0.29.

The large $\varepsilon^{1/3}$ peak at 17:05:14 has a double maximum spectrum (Fig. 10a). The pulse pair algorithm Eq.[3c] will fail under these conditions and will produce too large a value. The spectra, in general, have various shapes. The pulse pair algorithm is designed specifically for Gaussian shapes, however, sawtooth, flat-top, multimaxima as well as Gaussian shapes are observed. Consequently it is not surprising that perfect correlations are not observed. It is reasonable that an algorithm that takes into account the various shapes should be used. Many of the excessive values of $\varepsilon^{1/3}$ can be ascribed to either multi-modes or to flat-top spectra. The anomalous peak at 17:30:13 has a wide flat-top spectrum (Fig. 10b).

7.0 CONCLUSIONS, AND FUTURE PLANS

The spectral width ($\varepsilon^{1/3}$) is superior to the reflectivity in determining the presence of turbulence. The reflectivity is featureless compared to spectral width. The correlation between aircraft and radar $\varepsilon^{1/3}$ is not perfect and in general the radar $\varepsilon^{1/3}$ is higher and on occasion may be extreme. The extreme radar $\varepsilon^{1/3}$ values appear to be caused by flat-top or dual-maxima spectra.

Work is underway to design new algorithms that will take into account the spectral shape. Since the raw radar data has been recorded on tape, various algorithms are being tested to determine the one which results in the best correlation with the aircraft data. Comparisons between flights have to be made and an overall correlation coefficient has to be generated.

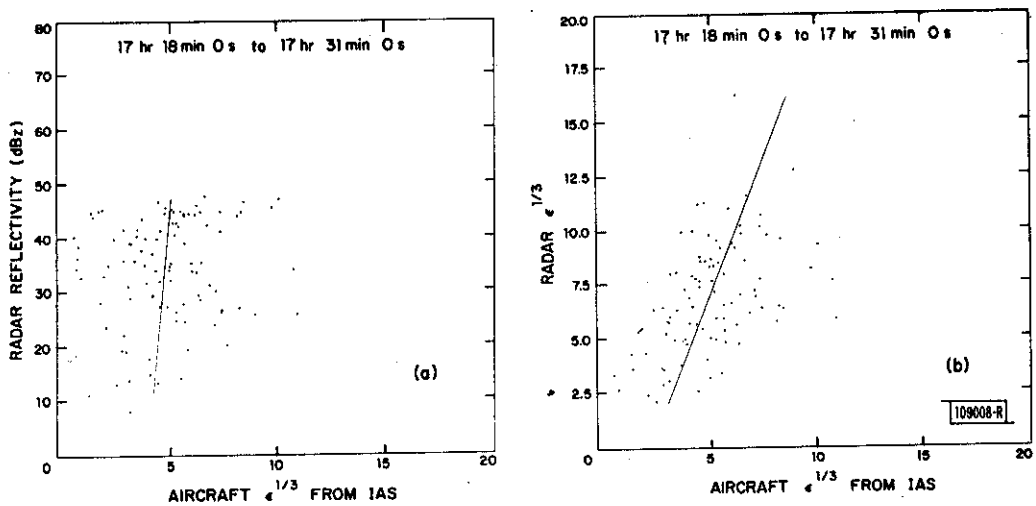

Fig. 9. (a-b) Scatter plots of radar $\epsilon^{1/3}$. (Flight of 17 July 1980). (a) Correlation coefficient = 0.48, (b) correlation coefficient = 0.097.

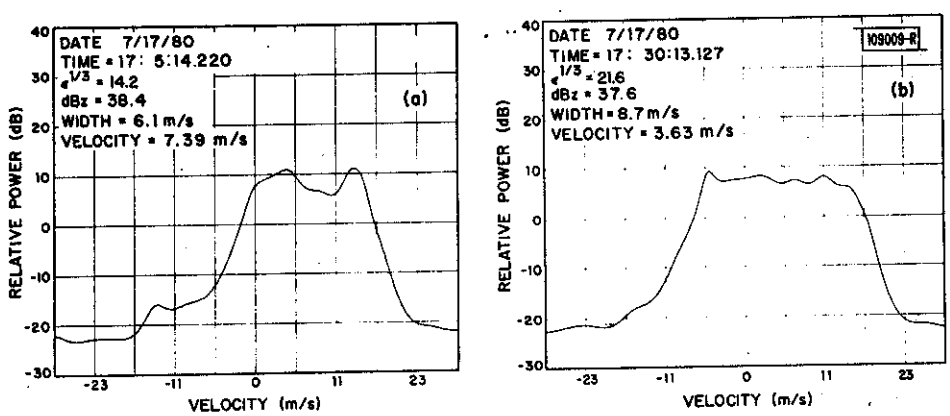

Fig. 10. Spectrum at two points having excessive radar $\epsilon^{1/3}$.

ACKNOWLEDGMENT

The direction and support of Mr. I. Goldman of the FAA Research and Development Service in the planning and execution of this program are gratefully acknowledged. Also, during the data-gathering phase of the program Mr. W. Lewis of the FAA Technical Center was of great assistance in coordinating the collection of data.

REFERENCES

1. J. T. Lee, "Application of Doppler Weather Radar to Turbulence Measurements Which Affect Aircraft," FAA Report RD-77-145 (March 1977).

2. R. T. Strauch, "Applications of Meteorological Doppler Radar for Weather-Surveillance Near Air Terminals", IEEE Trans. Geosci. Electron., G15-17, 4 (1979).

3. P. B. MacCready, "Standardization of Gustiness Values from Aircraft", J. Appl. Meteor. Vol. 3, 439 (1964).

4. S. Panchev, Random Functions and Turbulence (Pergamon Press, New York, 1971), p. 245.

5. A.S. Frisch and S.F. Clifford, "A Study of Convection Capped by a Stable Layer Using Doppler Radar and Acoustic Echo Sounders", J. Atmos. Sci. Vol. 31, 1622 (1974).

APPENDIX A

AIRCRAFT ACCELERATION STRUCTURE FUNCTION

The lift of an aircraft is given by

$$L = \frac{1}{2} C_L v^2 S$$

where

C_L = coefficient of lift,

ρ = air density,

v = aircraft true airspeed,

S = wing area.

The coefficient of lift, C_L, is a linear function of the angle of attack, over the range of interest. Therefore

$$L = \frac{1}{2} \left(\frac{u}{v} C_{L_\alpha}\right) \rho v^2 S$$

where C_{L_α} is the lift curve slope and u is the vertical component of airspeed. Thus

$$L = \frac{1}{2} C_{L_\alpha} \rho S u v$$

Taking differences we find

$$\Delta L = \frac{1}{2} C_{L_\alpha} \rho S [u\Delta v + v\Delta u]$$

Since $u \ll v$ and $(\Delta\mu)^2 \cong (\Delta v)^2$ we find

$$\Delta L \simeq \frac{1}{2} C_{L_\alpha} \rho S [v\Delta u]$$

and since the force $\Delta L = m\Delta a$ where m is the aircraft mass, we obtain for the acceleration difference

$$\Delta a = \frac{1}{2} C_{L_\alpha} \frac{\rho S}{m} v \Delta u$$

The structure function is defined as the average of the square of the differences

$$D_a = E\{(\Delta a)^2\} = \left(\frac{1}{2} C_{L_\alpha} \frac{\rho S}{m} v\right)^2 D_u$$

Kolmogorov's hypothesis* states that for lateral velocities

$$D_u = 4/3C(\epsilon r)^{2/3}$$

where C = universal constant (1.77)

ϵ = dissipation factor

r = separation distance when measuring the two velocities

However, $r = vt$ where t is the time difference between successive acceleration measurements. Therefore, we find for the square root of the acceleration structure function

$$\sqrt{D_a} = \frac{1}{\sqrt{3}} C_{L_\alpha} S C^{1/2} \rho \epsilon^{1/3} \frac{v^{4/3}}{m}$$

$$= KC^{1/2} \rho\epsilon^{1/3} \frac{v^{4/3}}{m}$$

For the Gulfstream

C_{L_α} = 5 (radians^{-1})

S = 610 square feet

m = 933 slugs

---

*S. Panchev, "Random Functions and Turbulence," Pergamon Press (1971) p. 151.

APPENDIX B

SOME BASIC RELATIONS CONCERNING THE RADAR MEASUREMENT OF AIR TURBULENCE

INTRODUCTION

The use of a radar to measure the level of air turbulence in a rain storm is a relatively new concept. Consequently, the purpose of this note is to present the connections between what a radar measures and the physical properties of the turbulent atmosphere. In the first section we will show that the radar spectrum represents the velocity distribution of the rain drops and appears to have a Gaussian shape. In the second section we will show how the radar spectrum width (variance) is related to the turbulence intensity and to the radar cell size.

SHAPE OF THE RADAR SPECTRUM

Consider a volume of scatterers such as rain drops that are being carried by a homogeneous, turbulent atmosphere. Let us look first at one of the rain drops. The radar return, in voltage, at time "t" and "t + τ" is proportional to:

$$e^{i\frac{4\pi\, x(t)}{\lambda}} \quad \text{and} \quad e^{i\frac{4\pi\, x(t+\tau)}{\lambda}} \tag{1}$$

where x is a random variable representing the position of the drop relative to the radar and λ is the radar wavelength. The correlation function of the return is by definition

$$\rho(\tau) = \frac{R(\tau)}{R(0)} = E\left\{e^{i\frac{4\pi\, x(t)}{\lambda}} \cdot e^{-i\frac{4\pi\, x(t+\tau)}{\lambda}}\right\} \tag{2}$$

$$= E\left\{e^{i\frac{4\pi}{\lambda}\left[x(t) - x(t+\tau)\right]}\right\}$$

$$= E\left\{e^{i\frac{4\pi}{\lambda} u\, \tau}\right\}$$

where

$$u \triangleq \frac{x(t) - x(t+\tau)}{\tau}$$

is a random variable representing the average velocity over the interval τ. "t" drops out because the statistics are assumed to be stationary. Evaluating (2) we find

$$\rho(\tau) = E \{ e^{i\frac{4\pi}{\lambda}u\tau} \} = \int_{-\infty}^{\infty} p(u)\ e^{i\frac{4\pi}{\lambda}u\tau}\ du. \tag{3}$$

Here p(u) is the probability density of u. However,

$$\rho(\tau) = \frac{1}{2\pi} \int_{-\infty}^{\infty} S(\omega)\ e^{i\omega\tau}\ d\omega \tag{4}$$

where $S(\omega)$ is the spectrum observed by the radar. Equating (3) and (4) we find

$$S(\omega)\ e^{i\omega\tau}\ d\omega = 2\pi\ p(u)\ e^{i\frac{4\pi}{\lambda}u\tau}\ du.$$

We see that

$$\omega = \frac{4\pi}{\lambda}u \quad \text{and} \quad \frac{d\omega}{du} = \frac{4\pi}{\lambda} \tag{4a}$$

and find that

$$S(\omega)d\omega = 2\pi p(u)du \text{ and } S(\omega) = \frac{\lambda}{2}p(u). \tag{5}$$

Thus, we see that the spectrum is a replica of the probability density of the velocity averaged over the interval τ. Because the spectra of independent processes can be added, Eq. (5) is valid for many raindrops, if one assumes all the droplet cross sections are the same.

It is not difficult to generalize Eq. (5) for varying droplet sizes. The return at time t for N droplets is

$$\sum_{n=1}^{N} A_n\ e^{i\frac{4\pi}{\lambda}x_n(t)}$$

where A_n is the amplitude of the nth droplet. The covariance function is

$$R(\tau) = E \{ \sum_{i=1}^{N} A_i\ e^{\frac{i4\pi x_i(t)}{\lambda}} \cdot \sum_{j=1}^{N} A_j\ e^{\frac{i4\pi x_j(t+\tau)}{\lambda}} \}.$$

Separating out the terms where i = j, we have

$$R(\tau) = E \{ \sum_{n=1}^{N} A_n^2\ e^{i\frac{4\pi}{\lambda}u_n\tau} + \sum_{j=1}^{N} \sum_{\substack{i=1 \\ j\neq i}}^{N} A_i A_j\ e^{i\frac{4\pi}{\lambda}(x_i - x_j)} \}.$$

Remembering that if two random variables (rv's) are independent, the expectation of the product of two rv's is the product of the expectations, we find

$$R(\tau) = N \; E\{A^2\} \; E\{e^{i\frac{4\pi}{\lambda} u\tau}\}$$

and

$$R(0) = N \; E\{A^2\}$$

Since x_i and x_j are independent, the cross terms drop out because

$$E\{e^{i\frac{4\pi}{\lambda}(x_i - x_j)}\} = E\{e^{i\frac{4\pi}{\lambda} x_i}\} \; E\{e^{i\frac{4\pi}{\lambda} x_j}\} = 0 \text{ when } j \neq i. \qquad (6)$$

Thus

$$\frac{1}{2\pi} \int_{-\infty}^{\infty} S(\omega) \, e^{i\omega\tau} \, d\omega = \rho(\tau) = \frac{R(\tau)}{R(0)} = E\{e^{i\frac{4\pi}{\lambda} u\tau}\}$$

$$= \int_{-\infty}^{\infty} p(u) \, e^{i\frac{4\pi}{\lambda} u\tau} \, du$$

or as before

$$S(\omega) = \frac{\lambda}{2} \; p(u). \qquad (5)$$

Thus, the "radar" spectrum is a replica of the velocity probability density. There appears to be some theoretical justification[1] for the velocity distribution to be Gaussian. Experimentally, in homogeneous turbulence, the velocity distribution is symmetric and tends to be nearly Gaussian[1,2,3]. It should be pointed out that in a related process, the motion of a molecule in a gas, that the distribution of one component of the velocity is Gaussian and is known as a Maxwellian distribution.

VARIANCE OF THE RADAR SPECTRUM

We have just established that the radar spectrum is a copy of the velocity distribution. It follows from Eq. (4a) that the variance of the radar spectrum σ_ω^2 is related to the velocity variance σ_u^2 as follows:

$$\sigma_\omega^2 = \left(\frac{4\pi}{\lambda}\right)^2 \sigma_u^2$$

We will now show how σ_u^2 (or σ_ω^2) is related to the air turbulence dissipation factor ε.

The variance σ_u^2 is by definition equal to

$$\sigma_u^2 = E\{(u - E\{u\})^2\}$$

$$= E\{u^2\} - (E\{u\})^2$$

where the expectation value $E\{\ \}$ is generally taken to mean an average over ensembles. However, the radar takes an average not over ensembles but over the radar cell volume. If the statistics are stationary over the volume, then volume averaging is the same as a sampled average. Therefore, a sampled value of the function "f" is

$$\langle f \rangle = \int A(\vec{r})\ f\ d\vec{r}$$

where

$$\int A(\vec{r})\ d\vec{r} = 1, \text{ and } d\vec{r} \text{ is a differential volume.}$$

$A(\vec{r})$ is the cell size and is closely approximated by

$$A(\vec{r}) = \frac{1}{(2\pi)^{3/2}\ b\ a^2}\ e^{-\left[\frac{y^2 + z^2}{2\ a^2} + \frac{x^2}{2\ b^2}\right]}.$$

We are assuming a cylindrical antenna beam of width "a" and a pulse length "b". Thus, a sampled value of the variance would be

$$\langle \sigma_u^2 \rangle = \langle u^2 \rangle - \langle u \rangle \langle u \rangle$$

or

$$\langle \sigma_u^2 \rangle = \int A(\vec{r})\ u^2(\vec{r})\ d\vec{r} - \int A(\vec{r}_1)\ u(\vec{r}_1)\ d\vec{r}_1 \int A(\vec{r}_2)\ u(\vec{r}_2)\ d\vec{r}_2$$

We find σ_u^2 by taking the expectation of the sampled average $\langle \sigma_u^2 \rangle$

$$\sigma_u^2 = \int A(\vec{r})\ E\{u^2\}\ d\vec{r} - \iint A(\vec{r}_1)\ A(\vec{r}_2)\ E\{u(\vec{r}_1)\ u(\vec{r}_2)\}\ d\vec{r}_1\ d\vec{r}_2.$$

Since $E\{u^2\}$ is not a function of $\vec{r}$ and $u(\vec{r}_1)$ and $u(\vec{r}_2)$ are correlated, we have

$$\sigma_u^2 = E\{u^2\} - \iint A_1(\vec{r}_1)\, A(\vec{r}_2)\, B_{\ell\ell}(\vec{r}_1, \vec{r}_2)\, d\vec{r}_1\, d\vec{r}_2 \tag{7}$$

where $B_{\ell\ell}(\vec{r}_1, \vec{r}_2)$ is the correlation of the two longitudinal velocities at points $\vec{r}_1$ and $\vec{r}_2$. Because the turbulence is assumed homogeneous

$$B_{\ell\ell}(\vec{r}_1, \vec{r}_2) = B_{\ell\ell}(\vec{r}_1 - \vec{r}_2).$$

Since $B_{\ell\ell}$ is a correlation, it can be defined in terms of a 3-dimensional Fourier transform

$$B_{\ell\ell}(\vec{r}_1 - \vec{r}_2) = \int \Phi_{\ell\ell}(\vec{k})\, e^{i\vec{k}\cdot(\vec{r}_1 - \vec{r}_2)}\, d\vec{k}.$$

The energy spectrum of the 3 dimensional velocity field $\Phi(\vec{k})$ is often confused with the radar Doppler spectrum $S(\omega)$. $\Phi_{\ell\ell}(\vec{k})$ follows an inverse 11/3 power law[4,5] and has a pole at the origin while $S(\omega)$ is gaussian-shaped. $\Phi(\vec{k})$ is the velocity spectrum while $S(\omega)$ represents the velocity distribution. ω has the dimensions of radians/second while $\vec{k}$ is radians/meter. The function $\Phi_{\ell\ell}(\vec{k})$ is known when the turbulence is isotropic and in the inertial subrange. We should notice that

$$E\{u^2\} = B_{\ell\ell}(0) = \int \Phi_{\ell\ell}(\vec{k})\, d\vec{k}$$

consequently, Eq. (7) becomes

$$\sigma_u^2 = \int \Phi_{\ell\ell}(\vec{k})\, d\vec{k} - \iint A(\vec{r}_1)\, A(\vec{r}_2) \int \Phi_{\ell\ell}(\vec{k})\, e^{i\vec{k}\cdot(\vec{r}_1 - \vec{r}_2)}\, d\vec{k}\, d\vec{r}_1\, d\vec{r}_2$$

$$\doteq \int \Phi_{\ell\ell}(\vec{k}) \left[1 - \int A(\vec{r}_1)\, e^{i\vec{k}\cdot\vec{r}_1}\, d\vec{r}_1 \int A(\vec{r}_2)\, e^{-i\vec{k}\cdot\vec{r}_2}\, d\vec{r}_2 \right] d\vec{k} \tag{8}$$

Evaluating the inner integral, by changing to rectangular coordinates, we have

$$\int A(\vec{r}_1)\, e^{i\vec{k}\cdot\vec{r}_1}\, d\vec{r}_1 =$$

$$\frac{1}{(2\pi)^{3/2}\, b\, a^2} \iiint e^{-\left[\frac{y^2 + z^2}{2a^2} + \frac{x^2}{2b^2}\right]}\, e^{i(k_x x + k_y y + k_z z)}\, dx\, dy\, dz$$

$$= \frac{1}{(2\pi)^{3/2} b\, a^2} \int_{-\infty}^{\infty} e^{-\frac{y^2}{2a^2} + i k_y y}\, dy \int_{-\infty}^{\infty} e^{-\frac{z^2}{2a^2} + i k_z z}\, dz \int_{-\infty}^{\infty} e^{-\frac{x^2}{2b^2} + i k_x x}\, dx$$

$$= e^{-\frac{1}{2}\left[k_x^2 b^2 + k_y^2 a^2 + k_z^2 a^2\right]}.$$

Therefore, Eq. (8) becomes

$$\sigma_u^2 = \int \Phi_{\ell\ell}(\vec{k}) \left[1 - e^{-\left[k_x^2 b^2 + k_y^2 a^2 + k_z^2 a^2\right]}\right] d\vec{k}$$

For isotropic turbulence in the inertial subrange[4]

$$\Phi_{\ell\ell}(\vec{k}) = \frac{E(k)}{4\pi k^2}\left(1 - \frac{k_x^2}{k^2}\right).$$

where[5]

$$E(k) = \alpha\, \varepsilon^{2/3} k^{-5/3}$$

$$k^2 = k_x^2 + k_y^2 + k_z^2$$

$$k = |\vec{k}|$$

$$\alpha = 1.35 \pm .06 \text{ (dimensionless)}^{6}$$

and

$$\varepsilon = \text{the dissipation factor.}$$

Substituting and using the following relations

$$k_x^2 = k^2 \cos^2\phi$$

$$d\vec{k} = k^2 \sin\phi \; dk\, d\phi \; d\theta,$$

we convert Eq. (8) to polar coordinates

$$\sigma_u^2 = \frac{\alpha\, \varepsilon^{2/3}}{4\pi} \int_0^{\pi} \int_0^{\infty} \int_0^{2\pi} k^{-5/3} \sin^3\phi \left[1 - e^{-k^2\{a^2 \sin^2\phi + b^2 \cos^2\phi\}}\right] d\theta\, dk\, d\phi$$

$$= \frac{\alpha\varepsilon^{2/3}}{2} \int_0^{\pi} \sin^3\phi \int_0^{\infty} k^{-5/3} \left[1 - e^{-k^2\{a^2 \sin^2\phi + b^2 \cos^2\phi\}}\right] dk\, d\phi.$$

Using the following solution[7] for the inner integral

$$\int_0^\infty x^{\nu-1} (1 - e^{-\mu x^p}) \, dx = - \frac{1}{|p|} \mu^{-\frac{\nu}{p}} \Gamma \left(\frac{\nu}{p} \right)$$

we obtain

$$\sigma_u^2 = \frac{9}{8} \alpha \varepsilon^{2/3} \Gamma (5/3) \int_0^\pi \sin^3 \phi \, (a^2 \sin^2 \phi + b^2 \cos^2 \phi)^{1/3} \, d\phi$$

and using symmetry we find

$$\sigma_u^2 = \frac{9}{4} \alpha \varepsilon^{2/3} \Gamma (5/3) \int_0^{\pi/2} \sin^3 \phi \, (a^2 \sin^2 \phi + b^2 \cos^2 \phi)^{1/3} \, d\phi \tag{9}$$

Substituting $t = \cos^2 \phi$, we find

$$\sigma_u^2 = \frac{9}{8} \alpha \varepsilon^{2/3} \Gamma (5/3) \, a^{2/3} \int_0^1 (1 - t) \left(1 - \left[1 - \frac{b^2}{a^2}\right] t\right)^{1/3} t^{-1/2} \, dt.$$

Since we are dealing with real numbers, the integral is valid when

$$0 \leq \frac{b^2}{a^2} \leq 1.$$

The integral representation of the Gaussian hypergeometric function is given by[8]

$$F(a, b; c; z) = \frac{\Gamma (c)}{\Gamma (b) \, \Gamma (c-b)} \int_0^1 t^{b-1} (1-t)^{c-b-1} (1-tz)^{-a} \, dt$$

where $R_e(c) > R_e(b) > 0$.

Therefore,

$$\sigma_u^2 = \Gamma \left(\frac{2}{3} \right) \alpha (\varepsilon a)^{2/3} \, F \left(-\frac{1}{3}, \frac{1}{2}; \frac{5}{2}; 1 - \frac{b^2}{a^2}\right) \tag{10}$$

where $b^2 \leq a^2$

The hypergeometric series converges when $h^2 \leq 1$ and is given by the monotonic series.*

*All the terms after the first are negative. It can be shown that there are no maxima or minima when $0 \leq h \leq 1$.

$$F(-\tfrac{1}{3}, \tfrac{1}{2}; \tfrac{5}{2}; h) = 1 - \frac{h}{15} - \frac{h^2}{105} - \frac{5}{1701} h^3 - \ldots \qquad \left[h = 1 - \frac{b^2}{a^2}\right]$$

Since

$$F(-\tfrac{1}{3}, \tfrac{1}{2}; \tfrac{5}{2}; 0) = 1,$$

$$F(-\tfrac{1}{3}, \tfrac{1}{2}; \tfrac{5}{2}; 1) = \frac{12\,\Gamma(\frac{3}{2})\,\Gamma(\frac{4}{3})}{\Gamma(\frac{11}{6})} \simeq .917$$

and $0 \leq h \leq 1$

we find that

$$.917 \leq F(-\tfrac{1}{3}, \tfrac{1}{2}; \tfrac{5}{2}; h) \leq 1.$$

Consequently, the hypergeometric factor in Eq. 10 has little effect and that the approximation

$$\sigma_u^2 \simeq \Gamma(\tfrac{2}{3})\,\alpha\,(\varepsilon a)^{2/3}$$

is valid.

For the case when the beamwidth is smaller than the pulse length

$$0 \leq \frac{a^2}{b^2} \leq 1,$$

we can substitute

$$t = \sin^2 \phi$$

into Eq. 9 and find in the same manner as before

$$\sigma_u^2 = \Gamma(\tfrac{2}{3})\,\alpha\,(\varepsilon b)^{2/3}\,F(-\tfrac{1}{3}, 2; \tfrac{5}{2}; 1 - \frac{a^2}{b^2}). \tag{11}$$

The series $F(-\frac{1}{3}, 2; \frac{5}{2}; g) =$

$$1 - \frac{4}{15} g - \frac{8}{105} g^2 - \frac{32}{1701} g^3 - \ldots \qquad \left[g = 1 - \frac{a^2}{b^2}\right]$$

converges as before when $0 \leq g \leq 1$, is also monotonic, and is bounded by

$$\frac{27}{55} = .491 \leq F(-\tfrac{1}{3},\ 2;\ \tfrac{5}{2};\ g) \leq 1$$

Consequently, the approximation

$$\sigma_u^{\,2} \simeq \Gamma\left(\tfrac{2}{3}\right)\ \alpha(\varepsilon\, b)^{2/3}$$

is not always justified.

COMMENTS

In a typical radar the pulse length is usually smaller than the beamwidth and therefore Eq. 10 will apply. The spectral width, σ_u, will thus be proportional to $(\varepsilon\, a)^{1/3}$. Since the beamwidth is proportional to the radar range, and that the buffeting of an aircraft can be shown to be proportional to $\varepsilon^{1/3}$, we find by solving Eq. (10) for $\varepsilon^{1/3}$ that

$$\varepsilon^{1/3} = \frac{\sigma_u}{a^{1/3}} \quad \frac{1}{\left[\Gamma(2/3)\ \alpha\ F(-\tfrac{1}{3},\ \tfrac{1}{2};\ \tfrac{5}{2};\ 1 - \frac{b^2}{a^2}\ )\right]^{1/2}}$$

$$\simeq C\,\frac{\sigma_u}{R^{1/3}}$$

where R is the range to the turbulence and C is a constant. Thus the buffeting will be directly proportional to the spectral width as seen at the radar and inversely proportional to the cube root of the range.

The use of a Gaussian function to approximate the range dimension of the cell is reasonable if one considers the effect of convolving the impulse response of the radar receiver with the transmitted rectangular pulse shape. The effective pulse shape will be rounded and look like a Gaussian curve. This will be particularly true if the receiver bandpass is closely matched to the transmitted pulse. The use of a Gaussian curve to approximate the main-lobe of the antenna has long been used and is considered to be quite accurate.

The variance derivation assumes that (1) the turbulence is uniform throughout the cell, (2) we are in the inertial subrange, (3) the raindrops move with the wind, and (4) there is no wind-shear. These assumptions are valid because of the following reasons. (1) By using small radar cells, homogeneity

becomes more likely. This is accomplished by operating at shorter radar ranges and/or using narrower antenna beams. (2) The inertial subrange signifies that the effects of inertia override the effects of viscosity and of gravity. The inertial subrange scale extends from about a millimeter to about a kilometer. Consequently radar cells less than a kilometer long can be filled with homogeneous turbulence. (3) The horizontal velocity components of the rain are expected to follow the wind but not the vertical components. At most antenna elevation angles of interest (i.e., small elevation angles), the horizontal components will dominate. (4) First-order effects of wind-shear broadening can be taken into account by measuring the mean velocity of adjacent cells and subtracting out the effect.

In the above derivation of the radar spectrum variance, the approach is similar to that of Frisch and Clifford[11] with the following differences. It was not necessary to explicitly take the 3-dimensional Fourier transform $F_p(\vec{k})$ in $\vec{k}$ space of the antenna pattern. The universal constant α (A in the Frisch paper) is not .47 but 1.35. The solution of the case where the pulse length is longer than the beamwidth is in error.

REFERENCES

1. G. K. Batchelor, Theory of Homogeneous Turbulence (Cambridge University Press, New York, 1959), Chap. VIII, p. 169.

2. J. L. Lumley and H. A. Panofsky, Structure of Atmospheric Turbulence (Interscience Publishers, New York, 1964), p. 94.

3. H. Tennekes and J. L. Lumly, A First Course in Turbulence (M.I.T. Press, Cambridge, MA., 1972), p. 246.

4. G. K. Batchelor, Theory of Homogeneous Turbulence (Cambridge University Press, New York, 1959), Eq. 3.4.12.

5. G. K. Batchelor, Theory of Homogeneous Turbulence (Cambridge University Press, New York, 1959), Eq. 6.5.3.

6. S. Panchev, Random Functions and Turbulence (Pergamon Press, New York, 1971), p. 245.

7. J. S. Gradshteyn and I. M. Ryzhik, Tables of Integrals Series and Products (Academic Press, New York, 1965), Formula 3.478, p. 342.

8. M. Abramowitz and I. A. Stegun, Handbook of Mathematical Functions NBS (U.S. Government Printing Office, Washington, 1964), Formula 15.3.1, p. 558.

9. R. R. Rogers and B. R. Trip, "Some Radar Measurements of Turbulence in Snow", J. Appl. Meteorol., Vol. 3, 603 (1964).

10. R. R. Rogers, "Radar Measurement of Velocities of Meteorological Scatterers", J. Atmos. Sci., Vol. 20, 170 (1963).

11. A. S. Frisch and S. F. Clifford, "A Study of Convection Capped by a Stable Layer Using Doppler Radar and Acoustic Echo Sounders", J. Atmos. Sci. Vol. 31, 1622 (1974).

12. R. C. Srivastava and D. Atlas, "The Effect of a Finite Radar Pulse Volume on Turbulence Measurements", 15th Radar Meteorological Conference, Tucson, AR, (Oct. 1972) p. 297.

APPENDIX C

AIRCRAFT MEASUREMENT OF $\varepsilon^{1/3}$

The following parameters are available on the Gulfstream aircraft to measure turbulence

P_f = Static or free stream pressure

Δp = Pitot tube differential pressure

T_t = Stagnaation or total temperature

P_f is taken from the static port of the pitot tube. $\Delta p = P_t - P_f$, where P_t is the total or stagnation pressure. Isentropic and ideal gas flow conditions are assumed permitting the following relations to be used.

$$\frac{P_t}{P_f} = \left(1 + \frac{\gamma-1}{2} M^2\right)^{\frac{\gamma}{\gamma-1}} \tag{1}$$

$$\frac{T_t}{T_f} = 1 + \frac{\gamma-1}{2} M^2 \tag{2}$$

$$M^2 = \frac{u^2}{\gamma R T_f} \tag{3}$$

Here M is the Mach number, γ is the ratio of specific heats, R is the gas constant, and u is the free stream airspeed.

Combining (1) and (3) we have

$$\left(\frac{P_t}{P_f}\right)^{\frac{\gamma-1}{\gamma}} = 1 + \frac{\gamma-1}{2} \frac{u^2}{\gamma R T_f} \tag{4}$$

Even under conditions of heavy turbulence, the fluctuations of P_t, T_t, M and u will be small compared to their respective mean values. Consequently, we can take differentials of (4), substitute differences and we find

$$\left(\frac{P_t}{P_f}\right)^{-\frac{1}{\gamma}} \frac{\Delta p}{P_f} = \frac{u\Delta u}{RT_f} \tag{5}$$

The structure function D is defined as the expectation of the differences of successive measurements squared or

$$D_u(\tau) \triangleq E\{[u(t+\tau) - u(t)]^2\}$$

Therefore, we can rewrite (5) as

$$\left(\frac{P_t}{P_f}\right)^{-\frac{2}{\gamma}} \frac{D_{\Delta p}}{P_f^2} = \frac{u^2 D_u}{(RT_f)^2} \tag{6}$$

Kolmogorov's Hypothesis relates D_u to ε as follows:

$$D_u = C(\varepsilon u\tau)^{2/3} \tag{7}$$

where τ is the time between measurements and C is a universal constant. Combining (6) and (7) we find

$$\varepsilon^{1/3} = C^{-1/2} \tau^{-1/3} u^{-4/3} RT_f \left[\frac{P_t}{P_f}\right]^{-\frac{1}{\gamma}} \frac{\sqrt{D_{\Delta p}}}{P_f} \tag{8}$$

However, since the temperature sensor does not measure the free stream temperature T_f but the total temperature T_t, we must combine (1), (2) and (3) with (8) and finally find

$$\varepsilon^{1/3} = \frac{\left(\frac{RT_t}{\tau}\right)^{1/3} \left(\frac{\gamma-1}{2\gamma}\right)^{2/3} \sqrt{D_{\Delta p}}}{C^{1/2}\left(1 + \frac{\Delta p}{P_f}\right)^{\frac{\gamma+2}{3\gamma}} \left[\left(1 + \frac{\Delta p}{P_f}\right)^{\frac{\gamma-1}{\gamma}} - 1\right]^{2/3} P_f} \tag{9}$$

where Δp is taken to be the mean of the differential pitot tube pressure over the averaging period of the structure function.